Geophysical Prospecting

EAGE EUROPEAN ASSOCIATION OF GEOSCIENTISTS & ENGINEERS

Geophysical Prospecting, 2013, **61** (**Suppl. 1**), 561–571 doi: 10.1111/j.1365-2478.2012.01109.x

3D pseudo-seismic imaging of transient electromagnetic data – a feasibility study

G.Q. Xue[1]*, L.-J. Gelius[2], L. Xiu[3], Z.P. Qi[3] and W.Y. Chen[1]

[1]*Institute of Geology and Geophysics, Chinese Academy of Sciences, Beijing, 100029, China,* [2]*Department of Geosciences, University of Oslo, 0316 Oslo, Norway, and* [3]*College of Geology Engineering and Geomatics, Chang'an University, Xi'an, 710054, China*

Received September 2010, revision accepted June 2012

ABSTRACT

We investigate a pseudo-seismic approach based on the so-called inverse Q-transform as an alternative way of processing transient electromagnetic (TEM) data. This technique transforms the diffusive TEM response into that of propagating waves obeying the standard wave-equation. These transformed data can be input into standard seismic migration schemes with the potential of giving higher resolution subsurface images. Such images contain geometrical and qualitative information about the medium but no quantitative results are obtained as in model-based inversion techniques. These reconstructed images can be used directly for geological interpretation or in further constraining possible inversions. We extend the original Q-transform based on an electrical-source formulation to the case of a large-loop TEM source. Moreover, an efficient discrete version of the inverse of this modified Q-transform is presented using a regularization method. Application of this inverse transform to the measured TEM responses gives the corresponding pseudo-seismic data, which are input into a 3D migration scheme. We then use a 3D boundary element type of Kirchhoff migration to ensure high computational efficiency. This proposed method was applied to both synthetic data as well as field measurements taken from an engineering geology survey. The results indicate that the resolution of the TEM data is significantly improved when compared with standard apparent-resistivity plots, demonstrating that higher resolution 3D transient electromagnetic imaging is feasible using this method.

Key words: Transient electromagnetic field, Pseudo-seismic field, Inverse Q-transform, Kirchhoff integral method, 3D TEM imaging.

INTRODUCTION

The transient electromagnetic (TEM) method has been widely used in connection with grounded source exploration (Gunderson, Newman and Hohmann 1986), subsurface target mapping (Cheesann, Edwards and Chave 1987; Xue, Song and Yan 2004; Xue, Elzein Mohammed and Guo 2010; Xue, Yan and Cheng 2011a; Xue, Yan and Li 2011b) and tunnel prediction (Xue *et al*. 2007a). However, the resolution associated with the conventional TEM survey is relatively low compared with that of seismic methods. Recently pseudo-seismic transformation techniques have been developed to make the use of imaging techniques such as migration feasible. This again implies that the data can be mapped into a higher resolution electrical structural model in a rather quick manner. Fast qualitative imaging is important for in-field processing and makes it possible to change recording strategies while surveying. It can be easily applied to large data sets as part of a standard processing procedure and can serve as well-constrained geometrical input for further inversions.

Pseudo-seismic imaging of magnetotelluric (MT) data was first investigated by Levy, Oldenburg and Wang (1988). However, the use of pseudo-seismic imaging within TEM has not been reported much in the literature. The main challenge is to

*E-mail: qqxueguoqiang@hotmail.com

develop a technique that transforms the diffusive time-domain TEM field into a pseudo-seismic wavefield that obeys a regular wave equation. Lee and McMechan (1987) and Lee, Liu and Morrison (1989) derived a forward transform, referred to as the Q-transform, which relates the pseudo-seismic wavefield to the corresponding diffusive field within an electrical source formulation. Li, Xue and Song (2005) and Xue, Yan and Lie (2007b) developed a modified Q-transform to include the case of a large-loop TEM source and introduced its optimized inversion counterpart. Use of this inversion algorithm makes it feasible to stably transform the TEM field into its corresponding pseudo-wavefield. After such a data transform, sophisticated imaging techniques originally developed for seismic exploration can now be applied (Xue 2011b). This implies that the TEM technique will have the potential of producing higher resolution geometrical images of complex geological media than those obtained from the direct use of diffusive data without applying more advanced inversion approaches.

Zhdanov and his colleagues (Zhdanov 1988; Zhdanov, Matusevich and Frenkel 1988; Zhdanov and Keller 1994; Zhdanov, Traynin and Booker 1996; Zhdanov and Portniaguine 1997) formulated a different approach to migrating low-frequency diffusive EM fields. Their formulation was based on inversion of the residual field (e.g., difference between measured and modelled fields) under a minimum-energy flow condition.

In this paper, we focus on the migration of TEM data by using the extended Q-transform as proposed by Li *et al*. (2005) and Xue *et al*. (2007b) in combination with 3D Kirchhoff migration. The actual implementation of the imaging technique is based on a 3D boundary element approach to increase the computational speed. The proposed formulation was applied to both synthetic and real TEM data. It demonstrates the potential of giving higher resolution images of the geoelectric subsurface.

In the following, we first provide a brief description of a TEM field system. Next, we introduce the theory behind the pseudo-seismic transformation. We derive an imaging formulation based on the Kirchhoff method that can handle TEM pseudo-wavefields. We then demonstrate the concept of pseudo-seismic imaging of TEM data by applying the method to both 3D synthetic and field data sets. We compare the classical apparent resistivity results with our pseudo-seismic TEM images and demonstrate the superior quality of the latter in terms of resolution. We conclude by a brief discussion on the limitations of the proposed method, namely, the pseudo-seismic imaging approach is able to give higher resolution geometrical and qualitative reconstructions of the subsurface. If more precise quantitative results are to be obtained, inversion techniques must be applied.

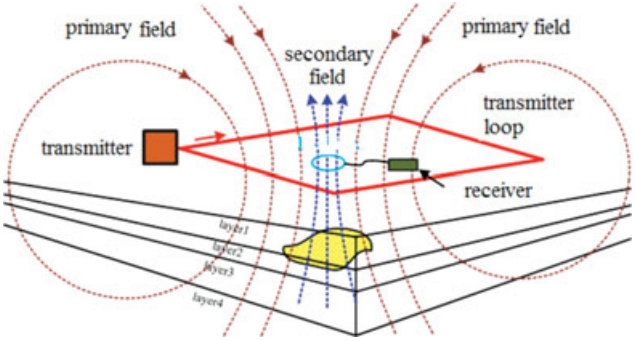

Figure 1 Sketch of a TEM field system.

BACKGROUND OF THE TRANSIENT ELECTROMAGNETIC FIELD SYSTEM AND METHOD

The central-loop TEM system consists in a transmitter loop and a receiver coil placed at the centre (Fig. 1). The transmitter loop is typically square and has 100–800 m side length. The transmitter current can vary from 1 Amps to as high as 400 Amps and commonly employs a ramp-off waveform. The rapid turn off of the current induces eddy currents in the ground, which in turn produce a secondary magnetic field measured by the receiver coil. The eddy currents diffuse as 'smoke rings' with time when the ground is homogeneous or layered. As time passes by, the current diffuses with distance at a rate that is related to the resistivity of the ground (Nabighian 1979; Kaufman and Keller 1983; Asten and Price 1985; Christiansen, Auken and Sørensen 2006).

Standard processing of large-loop TEM data involves transforming the recorded decay curves to apparent resistivity ρ_a. This quantity is derived from the late-time approximation of the impulse response as follows (Nabighian and Macnae 1991):

$$\rho_a(t) = \left\{ \frac{\pi\,(\mu_0/t)^5\, r^8}{400} \left| \frac{I}{U(t)} \right|^2 \right\}^{1/3}, \qquad (1)$$

where I is the transmitter current in Ampere, U is the measured voltage in Volt, t represents time in seconds, μ_0 is the permeability of the vacuum and r is the loop radius in metres (the loop area has to be converted into an equivalent circular area).

Apparent resistivity values calculated from equation (1) have the unit ohm-m and their variation with time defines the

apparent resistivity curve that can be employed to estimate the resistivity variations of the underground structure. However, this curve can not reveal clearly the geological boundaries because an apparent resistivity definition is a data normalization operation to convert the measured field quantities to a more understandable form of material resistivities. This fact has motivated the development of data interpretation approaches such as inversion and the pseudo-seismic imaging of TEM data presented in this paper. The inversion to recover resistivity distribution is a quantitative approach but is computationally expensive and can be time consuming. A migration approach, on the other hand, can be highly efficient and yield the desired structural information about the subsurface. Such an approach would be comparable to seismic migration, which can give higher resolution images of the subsurface from a qualitative and geometrical point of view.

WAVEFIELD TRANSFORMATION OF THE TRANSIENT ELECTROMAGNETIC FIELD

In this section we present the basic theory of the TEM-modified inverse Q-transform. Within an electrical source formulation, Lee and McMechan (1987) and Lee *et al.* (1989) established a relationship (Q-transform) between the pseudo-wavefield and the electric field intensity $E(t)$ that obeys the time-domain diffusion equation. By an analogy with this approach, it should also be possible to obtain the corresponding relationship between the pseudo-wavefield and the time-domain transient magnetic field response from a large-loop TEM source. The derivation of the relationship between these two types of fields is given in Appendix A and leads to the following TEM-type of Q-transform:

$$H_m(x, y, z, t) = \frac{1}{2\sqrt{\pi t^3}} \int_0^\infty \tau \, \exp[-\tau^2/4t] U(x, y, z, \tau) d\tau, \quad (2)$$

where $H_m(x, y, z, t)$ is a component of the TEM field, $U(x, y, z, \tau)$ represents the corresponding pseudo-wavefield and τ is the 'pseudo-time' of the pseudo-wavefield that is related to the actual time t of the TEM field. The discrete form of the above integral can be written as

$$H_m(x, y, z, t_i) = \sum_{j=1}^{n} U(x, y, z, \tau_j) a(t_i, \tau_j) h_j,$$
$$a(t_i, \tau_j) = \frac{1}{2\sqrt{\pi t_i^3}} \tau_j \, \exp\left[-\tau_j^2/4t_i\right], \quad (3)$$

where $a(t_i, \tau_j)$ is the kernel function that attenuates rapidly with increasing pseudo-time τ and h_j are the integral coefficients that will be determined.

By setting $U(x, y, z, \tau) = 1$ in equation (2) and introducing the same discrete representation as in equation (3), the integral will take the value (Anderson 1979)

$$\sum_{j=1}^{n} a(t_i, \tau_j) h_j = \frac{1}{\sqrt{\pi t_i}}. \quad (4)$$

The integral coefficients can now be computed from equation (4) for a given choice of a set of $\tau_j (j = 1, 2, ..n)$. However, since the time range of the TEM data is wide, each decay curve is divided into seven time ranges (gates) that are nearly equal on a logarithmic scale. These time intervals are (in ascending order): 32.5–80.0 μs, 80.0–325.0 μs, 325.0–800.0 μs, 800.0 μs – 2.4 ms, 2.4–8.7 ms, 8.7– 27.0 ms and 27.0–81.0 ms. For every time window the dimension n in equation (3) is selected as 20, thus 20 integral coefficients are obtained by solving equation (4). For further details about the integral coefficients the reader is referred to Table 1 in Xue *et al.* (2007b).

Having obtained these coefficients the pseudo-seismic wavefields are reconstructed from an inversion of equation (3) by the use of a combined optimization and regularization algorithm (see Appendix B for more details).

3D TRANSIENT ELECTROMAGNETIC PSEUDO-WAVE EQUATION IMAGING

It can be realized to transform the TEM field into its corresponding pseudo-wavefield by using an inverse Q-transformation algorithm and accordingly, a Kirchhoff integral of the TEM pseudo-wavefield can be developed for seismic data processing.

Kirchhoff integral of the transient electromagnetic pseudo-wavefield

The propagation of the pseudo-wavefield U in the subsurface that obeys a scalar wave equation can be described by:

$$\nabla^2 U - \frac{1}{v^2} \frac{\partial^2 U}{\partial t^2} = 0, \quad (5)$$

where v is the wave velocity.

Consider a closed 3D volume Ω defined by the boundary $Q = Q_0 + Q_1$ where Q_0 represents the portion of the boundary where the measurements are taken, i.e., the surface of the earth and Q_1 defines an artificial semispherical surface, as shown in Fig. 2. Letting the radius of the surface Q_1

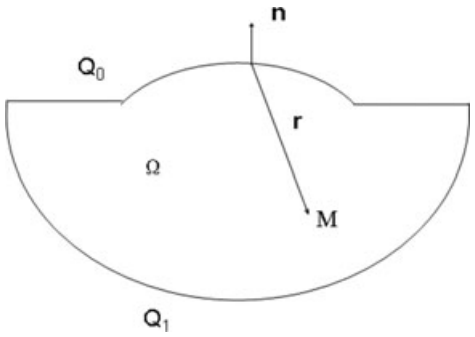

Figure 2 Region and boundary for downward extrapolation.

approach infinity, the pseudo-wavefield will take negligible values on this surface due to its asymptotic behaviour. If the pseudo-seismic scattered wavefields, U, on the surface, Q_0, are known, the corresponding upward travelling wavefields, w at an arbitrary depth position, $\vec{r}$ can be computed from the Kirchhoff-Helmholtz back propagation formula (Schneider 1978):

$$w\left(\vec{r}, t-\frac{R}{v}\right) = -\frac{1}{4\pi}\int\limits_{Q_0}\int\left\{\left[U(\vec{r}', t)\right]\frac{\partial}{\partial n}\left(\frac{1}{R}\right) - \frac{1}{R}\left[\frac{\partial U(\vec{r}', t)}{\partial n}\right] - \frac{1}{vR}\frac{\partial r}{\partial n}\left[\frac{\partial U(\vec{r}', t)}{\partial t}\right]\right\}d\vec{r}', \tag{6}$$

where $\partial/\partial n$ represents the derivative of the normal vector pointing outward and $R = |\vec{r} - \vec{r}'|$ is the distance between a subsurface point and a point on the measurement surface. The downward extrapolation formula in equation (6) can alternatively be written in the form

$$w(\vec{r}, t) = -\frac{1}{4\pi}\int\limits_{Q_0}\int\left\{\left[U\left(\vec{r}', t+\frac{r}{v}\right)\right]\frac{\partial}{\partial n}\left(\frac{1}{R}\right) - \frac{1}{R}\left[\frac{\partial U(\vec{r}', t+\frac{r}{v})}{\partial n}\right]\frac{1}{vR}\frac{\partial r}{\partial n}\left[\frac{\partial U(\vec{r}', t+\frac{r}{v})}{\partial t}\right]\right\}d\vec{r}', \tag{7}$$

where in the case of a layered subsurface model, the velocity v represents an RMS-average (or NMO-type) of the wave velocity by an analogy with seismic waves. A 3D boundary element solution of the integral in equation (7) is difficult to obtain in the seismic case since the vertical gradient $\partial u/\partial n$ can usually not be measured. However, in the case of TEM a gradient probe can be used.

A final image of the subsurface can be obtained by imposing a boundary condition. If a scatterer (or reflector) exists at a given subsurface location, the incident field and the time-reversed field must coincide in time. This can mathematically be described as a zero-lag cross-correlation between the two fields (Claerbout 1976):

$$image(\vec{r}) = \int H_i(\vec{r}, t')w(\vec{r}, t')dt', \tag{8}$$

where H_i is the modelled pseudo-seismic source (incident) field.

Boundary element method of wavefield continuation

It is easier to acquire vertical-gradient data in a TEM survey than a seismic exploration survey. Thus, the TEM wavefield transformed data can be downward extrapolated employing a 3D curved surface formulation. In order to solve integrals (7) over curved surfaces, the boundary element technique proves to be numerically efficient. This section will briefly discuss the implementation of the downward continuation in equation (7)) by employing the boundary element method (Li *et al.* 2005).

First, the boundary Q_0 should be divided into N^T elements so that equation (7) can be expressed as a summation over a series of element integrals:

$$w(x, y, z, t) = -\frac{1}{4\pi}\sum_{\alpha=1, N^T}\int\int_{\Gamma_\alpha}\left\{\frac{\partial}{\partial n}\left(\frac{1}{R}\right) - \frac{1}{R}\frac{\partial}{\partial n} - \frac{1}{vR}\frac{\partial r}{\partial n}\frac{\partial}{\partial t}\right\}U_\alpha\left(\xi, \eta, \zeta_0.t+\frac{R}{v}\right)d\Gamma_\alpha. \tag{9}$$

The boundary is discretized using triangular elements. As the element Γ_α is generally small, one may approximate the pseudo-wavefield U with linear interpolation:

$$U_\alpha = \sum_{\gamma=1}^{3}\xi_{\alpha\gamma}U_\gamma, \tag{10}$$

where U_γ represents the pseudo-wavefield at each of the three vertices, or nodes, of the triangular element and $\xi_{\alpha\gamma}, \gamma = 1, 2, 3$ represent the corresponding linear shape functions (Migeot *et al.* 2000).

Note first that $\frac{\partial R}{\partial n} = \cos(\hat{\boldsymbol{R}}\cdot \mathrm{n})$, where $\hat{\boldsymbol{R}}$ represents a unit vector along the direction of the distance $\boldsymbol{R}$ and $\mathbf{n}$ represents the vertical direction of 3D volume boundary. Making use of this result combined with equation (10), we can obtain an alternative form of equation (9):

$$w(x, y, z, t) = \frac{1}{4\pi}\sum_{\alpha=1}^{N^T}\left[\sum_{\gamma=1}^{3}\left(f_{\alpha\gamma}U_\gamma + d_{\alpha\gamma}\frac{\partial U_\gamma}{\partial n} + c_{\alpha\gamma}\frac{\partial U_\gamma}{\partial t}\right)\right], \tag{11}$$

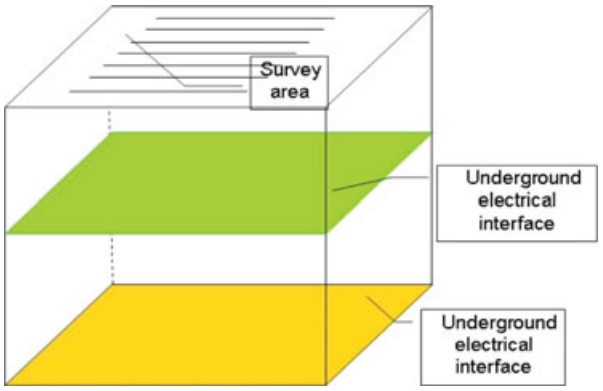

Figure 3 Three-layer geoelectric test model ($\rho_1 = 50$ ohm-m, $\rho_2 = 500$ ohm-m, $\rho_3 = 5000$ ohm-m, and $h_1 = 100$ m, $h_2 = 200$ m).

where

$$f_{\alpha\gamma} = \int_{\Gamma_\alpha}\int \xi_{\alpha\gamma}\frac{\cos(\hat{\mathbf{R}}\cdot\mathbf{n})}{R^2}d\Gamma_\alpha,\ d_{\alpha\gamma} = \int_{\Gamma_\alpha}\int \xi_{\alpha\gamma}\frac{1}{R}d\Gamma_\alpha,$$
$$c_{\alpha\gamma} = \int_{\Gamma_\alpha}\int \xi_{\alpha\gamma}\frac{\cos(\hat{\mathbf{R}}\cdot\mathbf{n})}{vR}d\Gamma_\alpha. \qquad (12)$$

The double summation in equation (11) can be seen as a loop over all the elements including a loop over the nodes belonging to each element. As shown by Migeot *et al.* (2000) this double sum can be permuted and replaced by a loop over all the nodes (n) including a loop over the elements in contact with that node (N^α):

$$w(x,y,z,t) = \frac{1}{4\pi}\sum_{\gamma=1}^{n}\left[\sum_{\alpha=1}^{N^\alpha}\left(f_{\alpha\gamma}U_\gamma + d_{\alpha\gamma}\frac{\partial U_\gamma}{\partial n} + c_{\alpha\gamma}\frac{\partial U_\gamma}{\partial t}\right)\right]$$
$$= \frac{1}{4\pi}\sum_{\gamma=1}^{n}\left[F_\gamma U_\gamma + D_\gamma\frac{\partial U_\gamma}{\partial n} + C_\gamma\frac{\partial U_\gamma}{\partial t}\right]. \qquad (13)$$

Finally, we assume that the nodes coincide with the actual measurement points so that the quantities are all known from the TEM experiment.

MODEL SIMULATIONS

In order to verify the feasibility of the proposed imaging method, we apply it to two synthetic data sets. First, a three-layer 1D geoelectric earth model was employed with parameter values (resistivity and thickness) as follows: $\rho_1 = 50$

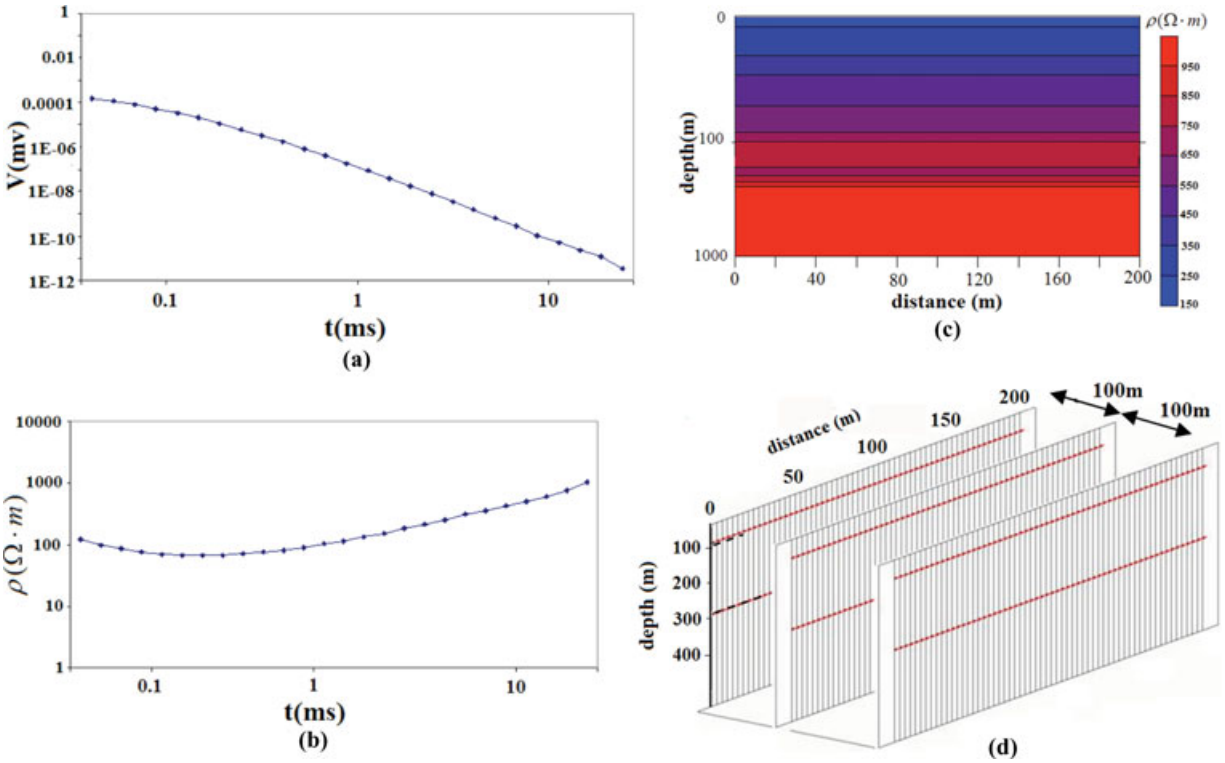

Figure 4 Results from 1D model simulation: (a) Secondary voltage decay curve. (b) Apparent resistivity-depth curve. (c) Apparent resistivity pseudosection. (d) Kirchhoff image based on pseudo-wavefield transformed TEM data.

ohm-m, ρ_2 = 500 ohm-m, ρ_3 = 5000 ohm-m and h_1 = 100 m, h_2 = 200 m (cf. Fig. 3). In the calculations a square-transmitter-loop of 200 m and a total of 11 survey lines (profiles) were assumed. Each survey line consists in 11 evenly spaced receivers (20 m apart) and the width of the time recording window was set to 32.5 μs–8.7 ms. The decay curves of the central-loop system corresponding to every survey point for this model have been calculated using software we implemented based on the method presented by Anderson (1979) and Asten *et al*. (1985) and are shown in Fig. 4(a). Conversion

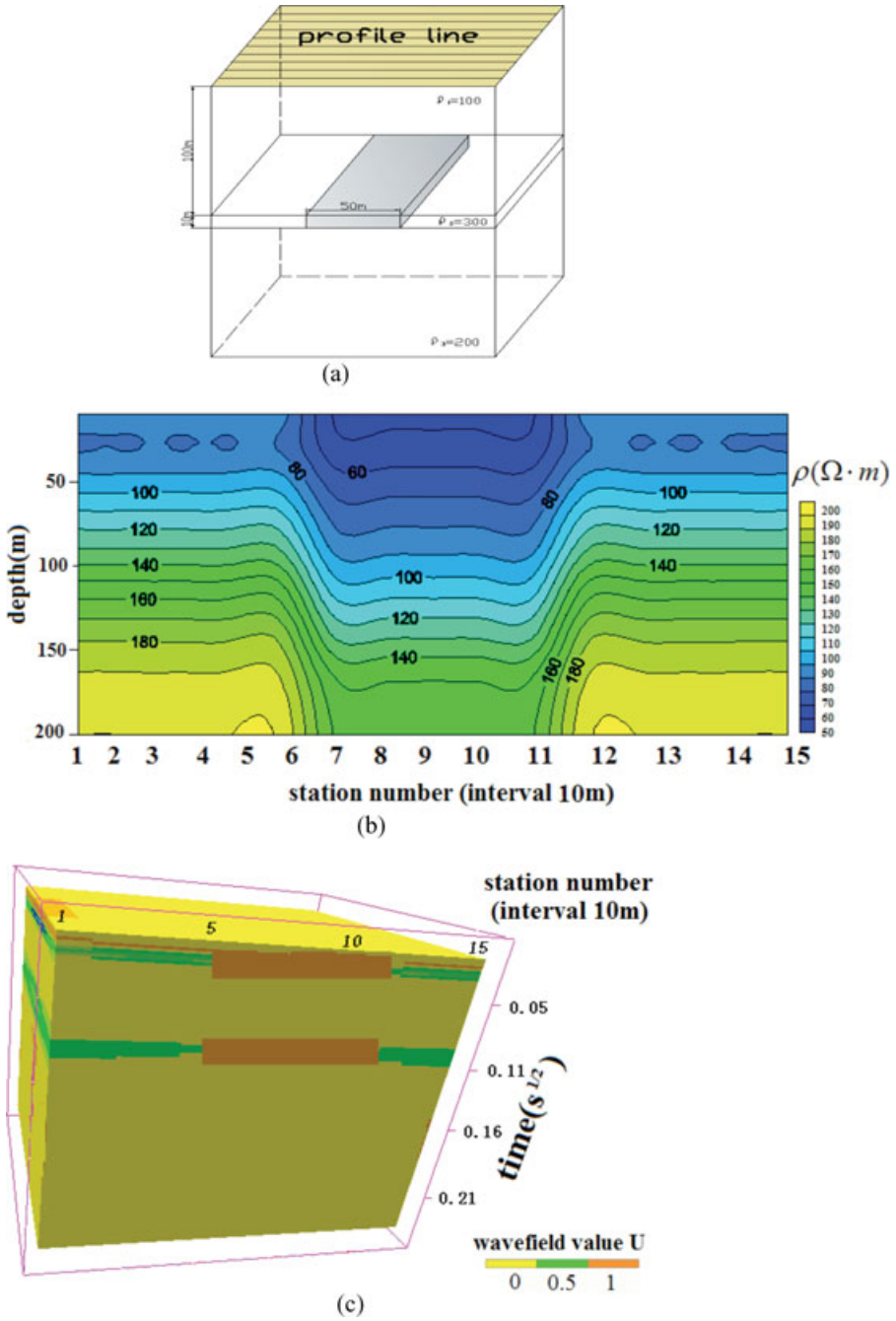

Figure 5 Results from 3D model simulation: (a) Test model including a 3D low-resistivity body. (b) Modelled apparent resistivity pseudosection. (c) Pseudo-transformed wavefields corresponding to all profiles and interpolated within a 3D cube. $s^{1/2}$ is the time unit of pseudo-transformed wave-field travel time.

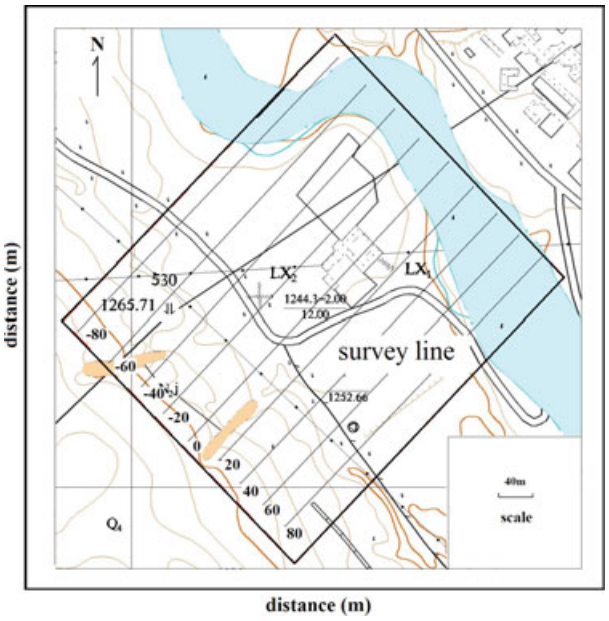

Figure 6 Map of the case-study area including survey layout.

to apparent resistivity as a function of time was obtained by use of equation (1) and conversion from time to depth (D) by using the following formula (Spies 1989):

$$D(t_i) = \sqrt{\frac{\rho_a t}{2\mu_0}}. \tag{14}$$

The corresponding apparent resistivity-depth curve is shown in Fig. 4(b). By calculating such curves for each receiver point along a given survey line and then interpolating, we obtain the result shown in Fig. 4(c). From this figure, it can be seen that the true geoelectric interfaces are not well imaged. Next, the same data were transformed to their pseudo-seismic equivalent before being input into the Kirchhoff time migration. A velocity analysis analogous to seismic processing was carried out to obtain the background velocity field. The final calculated result is shown in Fig. 4(d) represented by three vertical slices through the 3D imaged volume. The two geoelectric interfaces are now well recovered and also placed at the right depth.

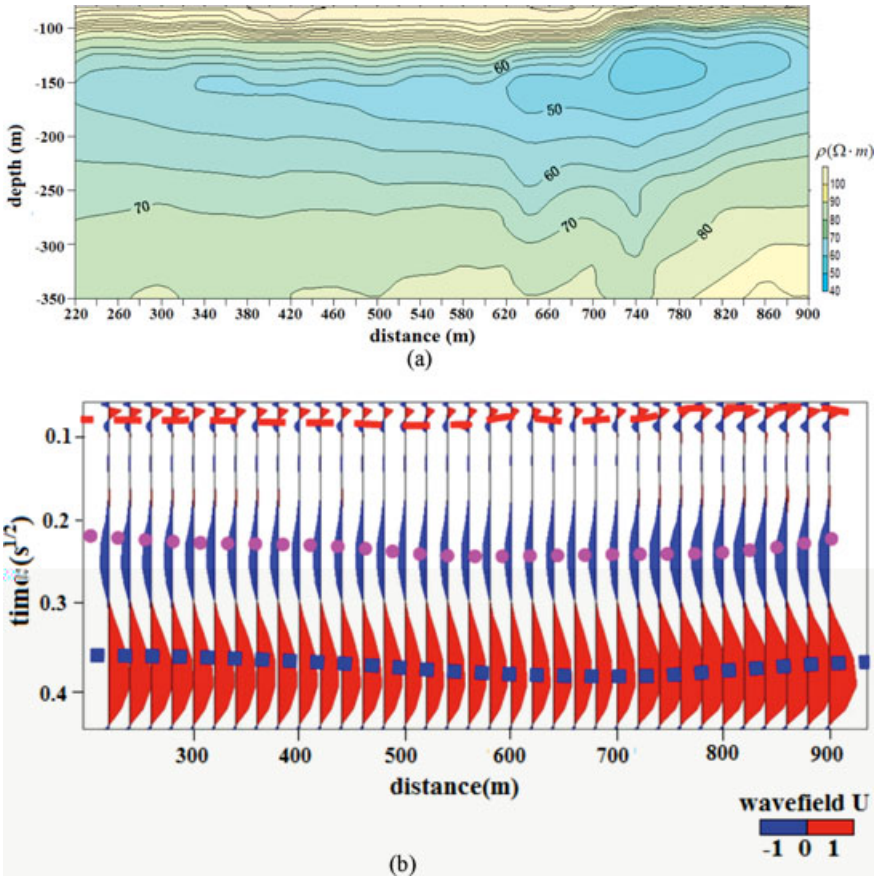

Figure 7 (a) Apparent resistivity pseudosection for survey line 0 (centre profile). (b) Corresponding pseudo-transformed wavefield response.

The second example represents a more realistic case involving a 3D conductive body embedded in a three-layer geoelectric background (cf. Fig. 5a). The parameters for the 1D layered background were chosen as: $\rho_1 = 100$ ohm-m, $\rho_2 = 300$ ohm-m, $\rho_3 = 200$ ohm-m, $h_1 = 100$ m and $h_2 = 10$ m. The second layer acted as the host layer for a 3D rectangular body with a thickness of 10 m, in-line dimension of 50 m and a cross-line dimension of 100 m. The resistivity of this body was set to 5 ohm-m. A total of 15 survey lines (20 m interval between each profile) were simulated and for each line 15 evenly spaced receiver positions (10 m apart) were assumed.

The apparent resistivity variation with depth corresponding to the centre profile is shown in Fig. 5(b). The lateral extent of the 3D target is well resolved but the vertical resolution is rather poor due to the diffusive character of the TEM field. Hence, the top and bottom of the body cannot be easily identified. Next, the synthetic TEM data set was transformed to its pseudo-wavefield form. By interpolating the pseudo-wavefields corresponding to each survey line the 3D cube shown in Fig. 5(c) could be constructed. The top and bottom of the 3D target is now well recovered and also its lateral extent. The actual migration is not shown here since it will virtually give the same type of result since all structural interfaces are horizontal.

APPLICATION TO FIELD DATA

We now apply our method to the processing of TEM data acquired in a mine safety application. It is well-known that many types of geological hazards exist in connection with mining. The hazards can occur in excavated areas, collapsing rock columns and isolated water bodies. The case study presented here was carried out at a coal mine in the Shanxi Province in China (cf. Fig. 6 showing a map and corresponding survey lines). The main purpose of the survey was to identify possible water-filled excavated regions in order to avoid an accident of water flooding during the current mining process.

The upper surface of the survey area is characterized by Quaternary loess with a thickness of no more than 20 m. The underlying strata consist of mainly Tertiary gritstone layers, Permian sand-mudstone intercalated by coal layers, Carboniferous sand-mudstone intercalated by coal layers and Ordovician limestone layers. Two main coal seam distributions exist in this area located at approximately 140 m and 260 m in depth respectively. Differences in resistivity between the different geological strata are small overall, except in areas that have already been excavated. In such regions the change in the stress situation causes the roof of the mined-out area to deform

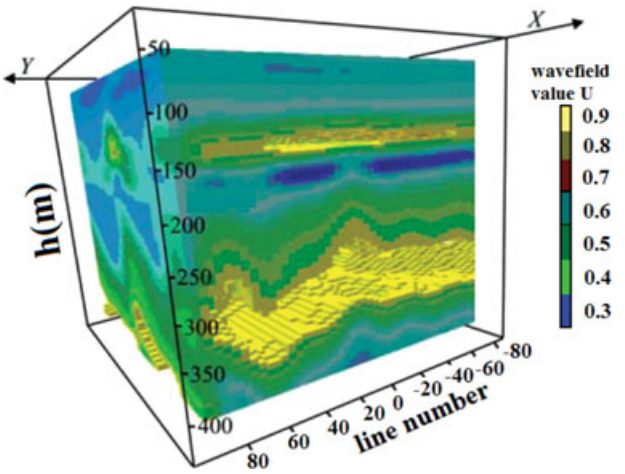

Figure 8 Kirchhoff image of the underground in the survey area.

and fracture. The creation of fault and bending zones leads to groundwater filling as well as leakage of water seeping from the surface along the cracks. As a consequence excavated regions after being water-filled will form low-resistance bodies that differ from the surrounding rock strata.

A central-loop configuration was employed in the current working area, the side length of the transmit loop was chosen to be 200 m and the line spacing was 20 m. The distance between each measurement point for a given line was also 20 m. The number of time gates was 40 with a time range between 0.087–10 ms. The employed instrument was a V8-network multi-function TEM system provided by the Canadian company Phoenix Geophysics Limited.

Figure 7(a) shows a contour plot of the apparent resistivity as a function of depth for survey line 0 (the centre survey line as shown in Fig. 6). Due to the diffusive TEM response this 'image' is rather smeared and it can be difficult even for a skilled interpreter to identify possible geoelectric interfaces. However, after applying the pseudo-wavefield transform to the TEM data associated with the same survey line, the results shown in Fig. 7(b) were obtained. Three main events can now be identified: a shallow high-resistance layer and two additional interfaces. After pseudo-transformation of all survey lines followed by 3D Kirchhoff migration, a 3D cube of the geological structure can be constructed after interpolation as shown in Fig. 8. Figure 9 shows an interpreted section corresponding to a vertical slice through the centre of the imaged 3D cubes (note that the vertical axis here represents altitude in metres and not directly depth). The two mined-out layers are assumed water-filled giving rise to the high-conductance response at altitudes of about 1100 m and 1010 m. This interpretation was later verified by drilling, demonstrating a high

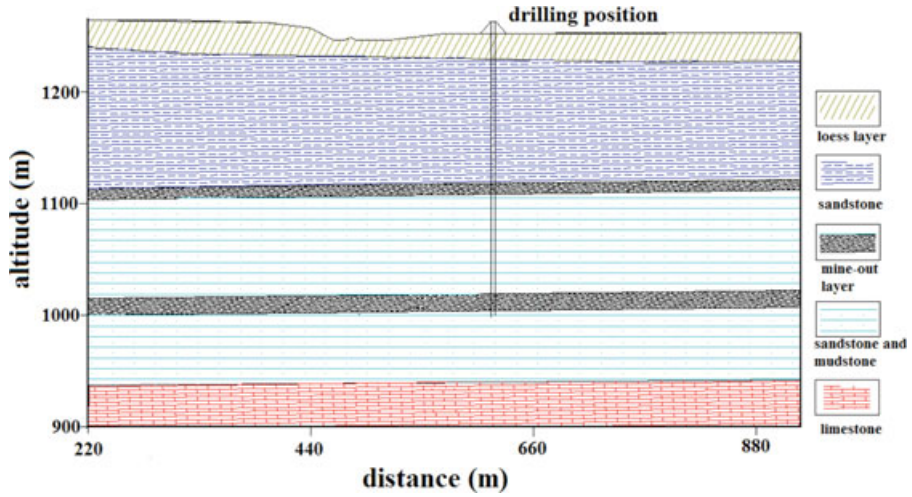

Figure 9 Interpretation based on a vertical slice through the centre of the image cube. The validity of this interpretation was later verified by drilling (well location given in the figure).

correlation with the actual geological findings and at the same time proving the effectiveness of the proposed qualitative technique.

CONCLUSIONS

By using an inverse TEM type of Q-transform, diffusive TEM field measurements can be converted to pseudo-wavefield data. The essence of this transform is to remove or dampen the dispersion and attenuation effects inherent in the recorded EM waves and enhance the propagation characteristics. These transformed data can be input into seismic migration in order to obtain images of the electric earth model. The feasibility of this data processing strategy was demonstrated in this paper by employing a 3D Kirchhoff-Helmholtz type of migration.

The performance of the proposed technique was tested on both synthetic TEM data and actual field recordings and produced good results. Compared with standard apparent-resistivity profiles, this new approach represents a feasible and practical way to increase the resolution capability of the TEM technique. Also, this new method can be used directly to fast imaging an underground 3D interface and there is no need to guess geo-electrical parameters as in normal 1D inversion

ACKNOWLEDGEMENTS

This research was financially supported by the Major State Basic Research Program of the People's Republic of China (2012CB416605). The authors would like to thank the Natural Science Foundation of China for support under grants 41174090 and 41174108. We also thank Principal Geophysicist Guangpin Li at Petroleum Geo-Services EM in Edinburgh for helpful suggestions to this manuscript. Finally, the authors would like to thank two anonymous reviewers and the Associate Editor A.T. Basokur for many helpful comments and suggestions.

REFERENCES

Anderson W.L. 1979. Computer Program: Numerical integration of related Hankel transforms of orders 0 and 1 by adaptive digital filtering. *Geophysics* **44**, 910–918.

Asten M.W. and Price D.G. 1985. Transient EM sounding by the in/out-loop method. *Exploration Geophysics* **16**, 165–168.

Cheesann S.J., Edwards R.N. and Chave A.D. 1987. On the theory of sea-floor conductivity mapping using transient electromagnetic system. *Geophysics* **52**, 204–217.

Christiansen A.V., Auken E. and Sørensen K. 2006. The transit electromagnetic method. In: *Groundwater resources in buried valleys. A challenge for geosciences*, pp. 65–76. Springer Verlag.

Claerbout J. 1976. *Fundamentals of Geophysical Data Processing*. McGraw-Hill Book Company.

Gfrerer H. 1987. An a-posterior parameter choice for ordinary and iterated Tikhonov regularization of ill-posed problems leading to optimal convergence rates. *Mathematics of Computation* **49**, 507–522.

Groetsch C.W. 1984. *The Theory of Tikhonov Regularization for Fredholm Equations of the First Kind*. Pitman Advanced Publishing Program.

Gunderson B.M., Newman G.A. and Hohmann G.W. 1986. Three dimensional transient electromagnetic responses for a grounded source. *Geophysics* **51**, 2117–2130.

Kaufman A.A. and Keller G.V. 1983. *Frequency and Transient Sounding: Methods in Geochemistry and Geophysics*. **16**. Elsevier Publishing Co.

Lee K.H., Liu G. and Morrison H.F. 1989. A new approach to modeling the electromagnetic response of conductive media. *Geophysics* **54**, 1180–1192.

Lee S. and McMechan G.A. 1987. Phase-field imaging: The electromagnetic equivalent of seismic migration. *Geophysics* **52**, 678–693.

Levy S., Oldenburg D. and Wang J. 1988. Subsurface imaging using magnetotelluric data. *Geophysics* **53**, 104–117.

Li X., Xue G.Q. and Song J.P. 2005. An optimized method for transient electromagnetic wave-field conversion. *The Chinese Journal of Geophysics (in Chinese)* **48**, 1185–1190.

Migeot J.-L., Meerbergen K., Lecomte C. and Coyette J.P. 2000. Practical implementation issues of acoustic BEM. In: *Boundary Elements Methods in Acoustics* (ed. O. von Estorff). Witpress.

Nabighian M.N. 1979. Quasi-static transient response of a conducting half-space – An approximate representation. *Geophysics* **44**, 1700–1705

Nabighian M.N. and Macnae J.C. 1991. Time-domain electromagnetic prospecting methods. In: *Electromagnetic Methods in Applied Geophysics – Theory*, Vol. II, part A (ed. M.N. Nabighian), pp. 427–520. Society of Exploration Geophysicists, Tulsa.

Schneider W. 1978. Integral formulation for migration in two dimensions or three dimensions. *Geophysics* **43**, 49–76.

Schock E. 1984. On the asymptotic order of accuracy of Tikhonov regularization. *Journal of Optimization Theory and Applications* **44**, 95–104.

Spies B.R. 1989. Depth of investigation in electromagnetic sounding method. *Geophysics* **54**, 872–888.

Xue G.Q., Elzein Mohammed E.A. and Guo W.B. 2010. The response of large-loop transient electromagnetic method. *University of Africa Journal of Science*, 1–17.

Xue G.Q., Song J. P. and Yan S. 2004. Detecting shallow cavity with TEF in China. *The Leading Edge* **25**.

Xue G.Q., Yan Y.J., and Cheng J.L. 2011a. Research on detection of 3D underground caves based on the TEM technique. *Environmental Earth Sciences* **64**, 425–430.

Xue G.Q., Yan Y.J. and Li X. 2007b. Pseudo-seismic wavelet transformation of transient electromagnetic response in geophysical exploration. *Geophysical Research Letters* **34**, L16405.

Xue G.Q., Yan Y.J. and Li X. 2011b. Control of Wave-Form Dispersion Effect and Applications in TEM Imaging Technique for Identifying Underground Objects. *Journal of Geophysics and Engineering* **8**, 195–201.

Xue G.Q., Yan Y.J., Li X. and Di Q.Y. 2007a. Transient Electromagnetic S-inversion in tunnel prediction. *Geophysical Research Letters* **34**, L18403.

Zhdanov M.S. 1988. *Integral Transforms in Geophysics*. Springer, Berlin.

Zhdanov M.S. and Keller G.V. 1994. *The Geoelectrical Methods in Geophysical Exploration*. Elsevier, Amsterdam.

Zhdanov M.S., Matusevich V.U. and Frenkel M.A. 1988. *Seismic and electromagnetic migration*. Nauka, Moscow (in Russian).

Zhdanov M.S. and Portniaguine O. 1997. Time-domain electromagnetic migration in the solution of inverse problems. *Geophysics*, **62**, 293–309.

Zhdanov M.S., Traynin P. and Booker J.R. 1996. Underground imaging by frequency domain electromagnetic migration. *Geophysics* **61**, 666–682.

APPENDIX A

DERIVATION OF THE PSEUDO-WAVEFIELD (Q)-TRANSFORM VALID FOR TEM DATA

Neglecting the displacement current in the conductive earth medium, the TEM magnetic field will satisfy the following diffusion equation:

$$\nabla \times \nabla \times \boldsymbol{H}_m(\boldsymbol{r}, t) + \mu\sigma \frac{\partial}{\partial t} \boldsymbol{H}_m(\boldsymbol{r}, t) = 0. \tag{A1}$$

By resemblance with equation (A1) introduce the potential function $\mathbf{U}(\mathbf{r}, \tau)$ that satisfies the following wave equation:

$$\nabla \times \nabla \times \boldsymbol{U}(\boldsymbol{r}, t) + \mu\sigma \frac{\partial^2}{\partial t^2} \boldsymbol{U}(\boldsymbol{r}, t) = 0, \tag{A2}$$

where the independent variable τ has the unit of the square root of time and the potential function $\mathbf{U}(\mathbf{r}, \tau)$ represents a wavefield propagating with a velocity of $\frac{1}{\sqrt{\mu\sigma}}$.

After a Laplace transformation, equations (A1) and (A2) take the form

$$\nabla \times \nabla \times \hat{\boldsymbol{H}}(\boldsymbol{r}, s) + \mu\sigma s \hat{\boldsymbol{H}}(\boldsymbol{r}, s) = 0, \tag{A3}$$

$$\nabla \times \nabla \times \hat{\boldsymbol{U}}(\boldsymbol{r}, p) + \mu\sigma p^2 \hat{\boldsymbol{U}}(\boldsymbol{r}, p) = 0, \tag{A4}$$

where,

$$\hat{\boldsymbol{H}}(\boldsymbol{r}, s) = \int_0^\infty \boldsymbol{H}_m(\boldsymbol{r}, t) e^{-st} dt \quad \text{and} \quad \hat{U}(r, p) = \int_0^\infty U(r, t) e^{-pt} dt. \tag{A5}$$

Assume now that $s = p^2$, so that equation (A3) becomes

$$\nabla \times \nabla \times \hat{\boldsymbol{H}}(\boldsymbol{r}, p^2) + \mu\sigma p^2 \hat{\boldsymbol{H}}(\boldsymbol{r}, p^2) = 0. \tag{A6}$$

Direct comparison between equations (A4) and (A6) gives:

$$\hat{\boldsymbol{H}}(\boldsymbol{r}, p^2) = \hat{\boldsymbol{U}}(\boldsymbol{r}, p). \tag{A7}$$

Omitting the space variable $\boldsymbol{r}$ without any loss of generality and stating the Laplace transformation explicitly gives an alternative form of equation (A7):

$$\int_0^\infty H_m(t) e^{-p^2 t} dt = \int_0^\infty U(\tau) e^{-p\tau} d\tau. \tag{A8}$$

Because $s = p^2$ this latter equation can be further simplified as

$$\int_0^\infty H_m(t)e^{-st}dt = \int_0^\infty U(\tau)e^{-\sqrt{s}\tau}d\tau. \quad \text{(A9)}$$

Finally, by taking an inverse Laplace transform on both sides of equation (A9) the following transformation from a (pseudo-)wavefield to a time-domain diffusive field can be obtained (Zhdanov 1988) :

$$H_m(t) = \frac{1}{2\sqrt{\pi t^3}}\int_0^\infty \tau e^{-\tau^2/4t}U(\tau)d\tau. \quad \text{(A10)}$$

In equation (A10), $H_m(t)$ now represents the TEM data and $U(\tau)$ the corresponding pseudo-seismic data.

APPENDIX B

REGULARIZATION METHOD

Equation (3) can be cast into the form of a matrix equation:

$$\vec{h} = A\vec{u}, \quad \text{(B1)}$$

where $\vec{h} = (H_{m,i})_n$ and $\vec{u} = (U_j)_n$ are values of the TEM field and the pseudo-wavefield, respectively and A is the coefficient matrix.

The solution of equation (B1) is unstable and ill-posed and Tikhonov regularization should be employed. First by rewriting equation (B1) as follows:

$$(A^T A)\cdot\vec{u} = A^T\vec{h}, \quad \text{(B2)}$$

its regularized form can be stated as

$$(A^T A + \alpha(\delta)I)\cdot\vec{u} = A^T\vec{h}, \quad \text{(B3)}$$

where A^T is the transposed coefficient matrix, I is the unit matrix and $\alpha(\delta)$ is the regularization parameter with δ representing the error between the computed and measured data.

Since the integration of equation (3) is divided into seven separate time intervals, the corresponding regularization parameter is then first found for each of these intervals. According to the regularization theory the parameter $\alpha(\delta)$ can be determined based on the deviation method (Groetsch 1984; Schock 1984; Gfrerer 1987). The formula describing the deviation error can be written as:

$$\Delta_\eta(\alpha) = \varphi(\alpha) - (\delta + \zeta\,\|U\|)^2, \quad \text{(B4)}$$

where $\varphi(\alpha) = \|AU - F\|^2$ is the squared error between the measured and modelled data. Quantities δ and ζ are the perturbation errors of respectively equation (B4) and the coefficient matrix A. An optimal solution can be achieved by directly setting the above error deviation to zero, which is

$$\Delta_\eta(\alpha) = \varphi(\alpha) - (\delta + \zeta\,\|U\|)^2 = 0. \quad \text{(B5)}$$

Equation (B5) can be solved by using the Newton iterative method (Groetsch 1984; Schock 1984; Gfrerer 1987). That is, we expand equation (B5) into a Taylor series around the α_k point (k^{th} iteration),

$$\Delta_\eta(\alpha) = \Delta_\eta(\alpha_k) + \Delta'_\eta(\alpha_k)\Delta\alpha_k = 0. \quad \text{(B6)}$$

where $\Delta'_\eta(\alpha)$ is the first-order derivative of $\Delta_\eta(\alpha)$.

For a given initial value $\alpha_0 > 0$ the following iterative Newton formulation can be established

$$\alpha_{k+1} = \alpha_k + \Delta\alpha_k = \alpha_k - \frac{\Delta_\eta(\alpha_k)}{\Delta'_\eta(\alpha_k)},\ k = 0, 1, 2, \ldots, n, \quad \text{(B7)}$$

where $\Delta\alpha_k$ represents the iteration step size. A suitable choice of the initial value will cause equation (B7) to converge quite rapidly.

After having determined the set of regularization parameters, equation (B3) is used to find the corresponding least-squares solution for the complete pseudo-seismic wavefield (Xue *et al*. 2007b).